Scale-free channeling patterns near the onset of erosion of sheared granular beds

Pascale Aussillous, Zhenhai Zou, Élisabeth Guazzelli, Le Yan, Matthieu Wyart

Scale-free channeling patterns near the onset of erosion of sheared granular beds

Pascale Aussillous[a], Zhenhai Zou[a], Élisabeth Guazzelli[a], Le Yan (晏乐)[b], and Matthieu Wyart[c,1]

[a]Aix-Marseille Université, CNRS, Institut Universitaire des Systèmes Thermiques Industriels, 13453 Marseille, France; [b]Kavli Institute for Theoretical Physics, University of California, Santa Barbara, CA 93106; and [c]Institute of Physics, École Polytechnique Fédérale de Lausanne, CH-1015 Lausanne, Switzerland

Edited by David A. Weitz, Harvard University, Cambridge, MA, and approved August 30, 2016 (received for review June 3, 2016)

Erosion shapes our landscape and occurs when a sufficient shear stress is exerted by a fluid on a sedimented layer. What controls erosion at a microscopic level remains debated, especially near the threshold forcing where it stops. Here we study, experimentally, the collective dynamics of the moving particles, using a setup where the system spontaneously evolves toward the erosion onset. We find that the spatial organization of the erosion flux is heterogeneous in space and occurs along channels of local flux σ whose distribution displays scaling near threshold and follows $P(\sigma) \approx J/\sigma$, where J is the mean erosion flux. Channels are strongly correlated in the direction of forcing but not in the transverse direction. We show that these results quantitatively agree with a model where the dynamics is governed by the competition of disorder (which channels mobile particles) and particle interactions (which reduces channeling). These observations support that, for laminar flows, erosion is a dynamical phase transition that shares similarity with the plastic depinning transition occurring in dirty superconductors. The methodology we introduce here could be applied to probe these systems as well.

gravel bed river | dynamical phase transition | plastic depinning

The response of erodible granular beds to shearing flows is of central importance in numerous natural phenomena such as sediment transport in rivers and estuaries, the evolution of mountains and landscapes, and the formation of dunes in the desert or underwater. The response also affects many engineering processes such as slurry transport in mining or petroleum industries. However, and despite more than a century of studies, there is still not a complete fundamental understanding of the process. One of the essential issues is to describe the onset of solid flow. The incipient motion of the grains is controlled by the Shields number, $\theta = \tau_b/(\rho_p - \rho_f)gd$, which is the shear stress τ_b induced by the fluid at the top of the bed scaled by the hydrostatic pressure difference across the grains of diameter d. Here ρ_p and ρ_f are the density of the solid and the fluid, respectively, and g is the acceleration due to gravity. One observes a critical Shields number θ^c below which motion stops (1), following a first transitory and intermittent regime in which the granular bed is continually reorganizing (2). This aging or armoring of the bed leads to a saturated state of the bed independent of its preparation (2–6). Once a stationary state is reached, the rate J of particle transport above this threshold follows $J \approx (\theta - \theta^c)^\beta$ with $\beta \in [1,2]$, as reviewed in ref. 7.

Several approaches have been introduced to describe these observations. Bagnold (8) and followers (9) emphasize the role of hydrodynamics. In their view, moving particles carry a fraction of the total stress proportional to their density m, such that the bed of static particles effectively remains at the critical Shields number. The hydrodynamic effect of a moving particle on the static bed is treated on average, which neglects fluctuations. Erosion–deposition models (2) are another kind of mean field description, which emphasize instead that moving particles can fill up holes in the static bed, leading to the armoring phenomenon described above. Deposition and erosion are modeled by rate equations, which implicitly assumes that the moving particles visit the static bed surface entirely. More recently, collective effects have been emphasized. In ref. 10, it was proposed that the erosion threshold is similar to the jamming transition that occurs when a bulk granular material is sheared (10). Finally, two of us (11) have proposed that the competing effects of bed disorder and interactions between mobile particles control the erosion onset.

New observations are required to decide which theoretical framework is most appropriate for the erosion problem, and for which conditions. In this article, we study, experimentally, the collective dynamical effects of the mobile particles near threshold, by measuring and averaging the trajectories of all of the grains on the top of the bed. Previously, a few studies have explored particle dynamics, but they have focused on isolated trajectories (2). Here, instead, we analyze the spatial organization of the erosion flux. We use a setup where the Shield number slowly and spontaneously decreases as erosion occurs, as also occurs in gravel rivers (12). This effect allows us to investigate precisely the approach to threshold. Strikingly, we find that, after averaging over time, the flux does not become homogeneous in space. Instead, fluctuations remain important, and particles follow favored meandering paths. As the threshold is approached from higher Shields numbers, we find that most of the erosion flux is carried only by a few channels within the bed. Quantitatively, the distribution $P(\sigma)$ of local flux σ in different channels is found to be extremely broad and to follow a power-law distribution $P(\sigma) \approx 1/\sigma$. Moreover, channels are uncorrelated in the direction transverse to the flow, but they display power-law correlations decaying as the inverse square root of the distance in the longitudinal direction. We perform a detailed comparison between these observations and the model introduced in ref. 11, and we find quantitative agreements for a wide range of flows spanning from the viscous to the inertial regimes. Our work thus demonstrates the key role of disorder and particle

Significance

The response of erodible granular beds to shearing flows controls numerous natural phenomena. A central aspect is the existence of a threshold stress below which erosion stops, and whose microscopic underpinning is debated. We use an experiment where this threshold is spontaneously reached to study the spatial organization of the erosion flux. We find that erosion is heterogeneous in space and occurs along favored channels whose distribution is extremely broad, with strongly anisotropic spatial correlations. These findings can be quantitatively explained by a model incorporating both the disorder of the static bed and the interactions between mobile particles, establishing a link between erosion and dynamical phase transitions known to occur in disordered environments.

Author contributions: P.A., É.G., and M.W. designed research; P.A., Z.Z., É.G., and L.Y. performed research; P.A., Z.Z., É.G., L.Y., and M.W. analyzed data; and P.A., É.G., L.Y., and M.W. wrote the paper.

The authors declare no conflict of interest.

This article is a PNAS Direct Submission.

[1]To whom correspondence should be addressed. Email: matthieu.wyart@epfl.ch.

This article contains supporting information online at www.pnas.org/lookup/suppl/doi:10.1073/pnas.1609023113/-/DCSupplemental.

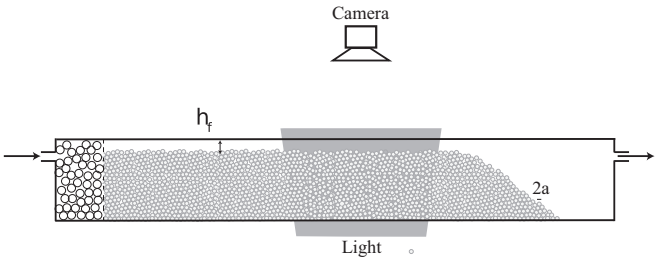

Fig. 1. Cross-section sketch of the experimental setup. The model flume apparatus consists of a rectangular perspex channel. It is filled with spherical particles of radius *a* while leaving an empty buffer space in the downstream region. When a constant flow rate is imposed, eroded particles fall out into the empty buffer space. This leaves an upstream region exhibiting a flat fluid–particle interface, the height *h* of which decreases with time until cessation of motion. A test section of this flat fluid–particle interface is imaged by a camera, and the real-time positions and velocities of the moving particles are collected.

interactions on the erosion threshold, and the need to use a framework that goes beyond mean field approaches. In addition, it opens ways to study dynamical phase transitions where both interactions and disorder are key, as is the case for the plastic depinning of vortices in dirty superconductors (13–15) or skyrmions (16), in a setting where table-top experiments can be performed.

Experimental Setup

In gravel-bed rivers, erosion occurs until the fluid stress at the top of the river bed reaches its threshold value (12, 17, 18). We use this effect and perform experiments in a model sediment river in which the Shield number continuously decreases as erosion occurs and eventually stops. In this setup, the distance to threshold can be accurately monitored by measuring the particle flux J, which slowly decreases with time until it vanishes.

We use a model flume apparatus consisting of a rectangular perspex channel (height 3.5 cm, width 6.5 cm, and length 100 cm; Fig. 1). We fill up the channel entrance with a granular bed of acrylic spherical particles (of radius $a = 1$ mm and density $\rho_p = 1.19$ g·cm^{-3}) while leaving an empty buffer space near the outlet. To cover both the viscous and inertial regimes of flows, this granular bed can be immersed in two different fluids, water (of viscosity $\eta = 1.0$ cP and density $\rho_f = 1.00$ g·cm^{-3}) and a mixture of water and UCON oil (of viscosity $\eta = 44.5$ cP and density $\rho_f = 1.06$ g·cm^{-3}). A given flow rate driven by a gear pump is then imposed and kept constant for the duration of each experimental run. At the inlet of the channel, the fluid flows through a packed bed of large spheres, providing a homogeneous and laminar flow. At the outlet, the fluid is run into a thermostated fluid reservoir, which ensures a constant temperature of 25 C° across the whole flow loop.

In this geometry, eroded particles fall out into the empty buffer space at the outlet. This leaves an upstream region exhibiting a flat fluid–particle interface, whose height decreases with time until cessation of motion. At constant fluid flow, θ decreases with the thickness of the fluid layer h_f (which increases with time) until the threshold of motion is reached from above (4). The experimental measurements are undertaken in the vicinity of the onset of motion, i.e., in a flow regime where only the particles located in the top one-particle-diameter layer of the bed are in motion; they consist of recording sequences of images of the top of the bed in a test section of the channel using a specially designed particle-tracking system (see details in *Methods*). The real-time positions and velocities of the moving particles are collected, and both local and total particles fluxes, σ and J, respectively, are inferred, as will be described in the following sections.

Channeling Pattern

Using particle tracking, the downstream and lateral velocities of each moving particle, u and v, respectively, are obtained. Time-averaging over all of the moving particles in the N processed images is then performed. The mean transverse velocity is found to be zero, whereas the mean downstream (or longitudinal) velocity is approximately constant for all of the runs for a given fluid (19). This is consistent with earlier findings that, as threshold is approached, the density m of moving particles vanishes, but not their average speed (2, 20, 21). Averaging over all runs yields a mean longitudinal velocity $U = 2.2$ mm/s for the water–Ucon mixture and $U = 36.1$ mm/s for water.*

From the measurement of these local particle velocities, the normalized local particle flux,

$$\sigma(i,j) = \frac{1}{N} \sum_{\text{particles}} (u/U), \qquad [1]$$

can be inferred at a given site (i,j) within a box having the size of one pixel in the image (one pixel is ~0.15 mm). Note that the sum of the normalized local velocities u/U is undertaken over all of the moving particles in the N processed images.

An example of the flux spatial organization $\sigma(i,j)$ is given in Fig. 2, *Left* as a grayscale level. One of our central findings is that, after time-averaging, the erosion flux is not uniform. Darker regions indicate paths that are more often visited by particles. Close to incipient motion, only a few channels are explored by the particles (see the first image of Fig. 2, *Left*). Farther from threshold, a greater number of preferential paths are followed, and, eventually, the particle trajectories cover the whole bed surface (see the third and fourth images of Fig. 2, *Left*).

Surface Visited by Moving Particles

We now quantify how the mean number of visited sites depends on the distance to the erosion threshold. The total normalized particle flux J is defined as the spatial average of the local particle flux σ over the N_{pixels} boxes in the image,

$$J = \frac{1}{N_{\text{pixels}}} \sum_{i,j} \sigma(i,j). \qquad [2]$$

Because the Shields number cannot be directly measured when the bed is viewed from above, the total flux J, which is a continuous function of the Shields number θ, is chosen as the control parameter of the experiment. As J increases, we find that the number of sites explored by the particles increases and eventually saturates when the whole surface of the test section is visited for a value $J_{\max} = 0.081$. Note that J can be seen as the surface concentration of the moving particles, and thus the saturation occurs when the mobile particles cover ~8% of the total surface. In Fig. 3, *Left*, the surface density of visited sites, ρ_{sites} (defined as the fraction of visited pixels in images such as those shown in Fig. 2), is plotted versus J. Interestingly, the data recorded in the viscous (×) and inertial (○) regimes (i.e., data obtained with the water–Ucon mixture and pure water, respectively) have the same trend and even are close to collapsing onto the same curve. Fig. 3, *Left*, *Inset* shows that the number of moving particles is linear in particle flux and vanishes at threshold for both the viscous and inertial data.

*This value of U can be simply recovered by balancing the drag force $C_D \rho_f \pi a^2 U^2/2$ on a particle with the friction force on the top of the bed $4\mu\pi a^3(\rho_p - \rho_f)g/3$, where $C_D = [24/Re_p][1 + 0.15 Re_p^{0.687}]$ is the Schiller–Naumann correlation for the drag coefficient with the particle Reynolds number defined as $Re_p = \rho_f a U/\eta$ and $\mu \approx 0.33$ is the friction coefficient, the value of which is in agreement with that found in previous work for suspensions (22, 23). The particle Reynolds number is $Re_p = 0.05$ for the water–Ucon mixture and is $Re_p = 36.10$ for pure water.

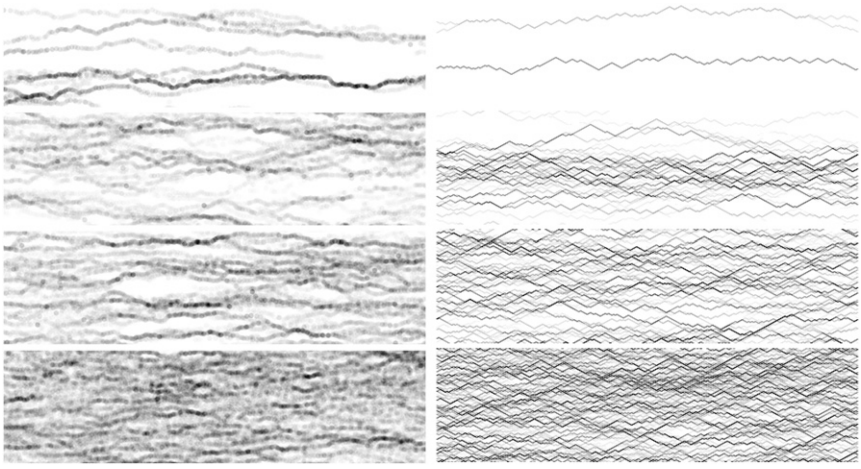

Fig. 2. Typical channeling patterns: (*Left*) experiments at $J/J_{max} = 0.09$, 0.35, 0.54, and 0.95 (from top to bottom), where $J_{max} = 0.081$, and (*Right*) model at $J/J_{max} = 0.18$, 0.25, 0.46, and 0.78 (from top to bottom), where $J_{max} = 0.25$. (*Left*) Experimental trajectories of the moving particles where the grayness indicates the magnitude of the local flux (see also Movies S1–S6 for both the pure water and the water–UCON mixture at different J/J_{max}). Darker paths correspond to paths that are more often visited by particles. (*Right*) The solid lines show the local fluxes σ along the edges, whose magnitudes measured in the steady state are indicated by the grayscale of the lines.

Distribution of Channel Strengths

To quantify the spatial organization of the erosion flux, we compute the distribution $P(\sigma)$ of the local particle fluxes σ as J is varied. Our key findings are shown in Fig. 4, *Left* and are as follows:

i) Close to threshold, the different curves $P(\sigma,J)$ can be collapsed using the functional form $P(\sigma,J) = J\, f(\sigma)$. Such scaling collapse is reminiscent of a continuous critical point. Note that this collapse holds in the range of local flux σ probed experimentally, but it cannot hold always, because the distribution must integrate to 1, as discussed below.

ii) For both the viscous (×) and inertial (∘) regimes, the function $f(x)$ is well fitted by the function $1/x$ (solid lines in the graphs), leading to

$$P(\sigma)/J \propto \sigma^{-1}. \quad [3]$$

Such a broad distribution is characteristic of a channeling phenomenon, for which some sites are almost never visited, whereas others are visited very often. Eq. **3** has no scale, indicating that the channel pattern is a fractal object. Obviously, at large σ, this distribution is cut off, as shown in Fig. 4, *Upper Left*; this simply indicates that there is a maximum possible flux a site can carry, if particles have a finite speed. More surprisingly, Eq. **3**, together with the constraint that $P(\sigma)$ integrates to 1, indicates the presence of a cutoff $\sigma_{min} \approx e^{-1/J}$, a quantity so small, however, that it does not appear in our observations at small J. However, for $J/J_{max} \gtrsim 0.37$, the scaling form of Eq. **3** breaks down at small σ (Fig. 4, *Lower Left*).

Spatial Correlations of the Channel Network

We now turn to the analysis of the spatial correlations of the particle flux, defined as

$$C_T(\Delta j) = \langle \sigma(i,j)\sigma(i,j+\Delta j)\rangle_c / \langle \sigma(i,j)\sigma(i,j)\rangle_c, \quad [4]$$

$$C_L(\Delta i) = \langle \sigma(i,j)\sigma(i+\Delta i,j)\rangle_c / \langle \sigma(i,j)\sigma(i,j)\rangle_c, \quad [5]$$

in the transverse and longitudinal directions, respectively. Here the symbol $\langle \bullet \rangle$ indicates a spatial average, and $\langle xy\rangle_c \equiv \langle xy\rangle - \langle x\rangle\langle y\rangle$.

Fig. 5, *Left* shows that there is no correlation in the transverse direction beyond $\sim 2a$ (for smaller distances, we observe anticorrelations that become more prominent as J increases). By contrast, long-range correlations appear in the longitudinal direction beyond $\sim 2a$ (delimited by a dashed line in the graphs). For small J, the decay can be well represented by a power law, $(\Delta i/a)^{\alpha}$ with $\alpha \approx -0.5$ (solid line in the bottom graph), and is independent of J. This observation further supports that the channel pattern is fractal with no characteristic length scales. For larger J, the decay deviates from this law and becomes stronger with increasing J.

Theoretical Model

We now show that these observations quantitatively agree with a theory incorporating two ingredients: (*i*) the channeling induced by the disorder (resulting from the presence of an essentially static bed) and (*ii*) the interaction among mobile particles. Why the first ingredient implies the second can be argued as follows: The trajectory of a single mobile particle must, overall, follow the main direction of forcing, but it will meander because it evolves on a bed that is disordered and static. Thus, there are favored paths that particles follow. If there are several mobile particles, this effect of the disorder tends to channel particles together along these paths. If mobile particles were not interacting, nothing would stop this coarsening from continuing, and, eventually, all particles would be attracted to the same optimal path. Obviously, this scenario is impossible for a large system, as the density along the favored path would be much larger than unity. Particle interaction is thus key to limiting channeling. Interactions result in two effects: First, a mobile particle cannot move into a site already occupied by another particle. Second, another particle can push on a mobile one and can deviate the latter from its favored path.

In ref. 11, these effects were incorporated in a model where both space and time were discretized, and where inertial effects as well as long-range hydrodynamic interactions were neglected. The static bed is treated as a frozen background of random heights h_l, where l labels the different sites of a square lattice. A fraction n of the lattice sites are occupied by particles that can move under conditions discussed below. The direction of forcing is along the lattice diagonal, indicated by the arrow in Fig. 6. There are two inlet bonds and two outlet bonds for each node. Bonds $l \to m$ are directed in the forcing direction, and are characterized by a declination $\theta_{l\to m} = h_l - h_m$. For an isolated particle on site l, motion occurs if there is an outlet for which $\theta + \theta_{l\to m} > 0$, where θ is the magnitude of the forcing acting on all particles. Flow occurs along the steepest of the two outlets, resulting in

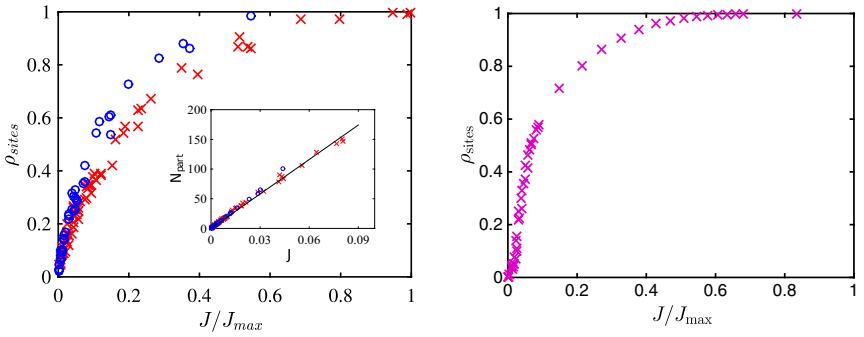

Fig. 3. Density of visited sites ρ_{sites} versus particle flux J scaled by the maximum value J_{max}: (*Left*) experiments using the water–UCON mixture (×) and pure water (○) and (*Right*) model. *Inset* on *Left* shows that the number of moving particles is linear in particle flux.

channeling. When particles move, they do so with a constant velocity; thus the flux J is simply the density of mobile particles, and is bounded by $J_{max} = n$ (the value of n does not affects the critical properties for $J \ll 1$; in Figs. 2–5, $n = 0.25$).

Finally, particles cannot overlap, but they can exert repulsive forces on particles below them. Such forces can untrap a particle that was blocked, but they can also deviate a moving particle from its course, as illustrated in Fig. 6. The path of a particle thus depends also on the presence of particles above it. As long as these features are present, we expect the model predictions to be independent of the details of the interactions. The detailed implementation of forces are presented in *Methods*.

Numerical Results

As shown in Fig. 2, the channeling map generated by the model reproduces qualitatively the experimental ones. Likewise, the dependence of the surface visited by mobile particles on the flux J shown in Fig. 3 closely matches experimental findings.

Our central result, however, is that this agreement is quantitative: The model predicts asymptotic behaviors that are consistent with observations. Although the range of flux and length scales available experimentally is smaller than in the model, the comparison is made with no fitting parameters and thus supports that the model is correct. First, as shown in Fig. 4, both the model and the experiment obtain the same form for $P(\sigma) \approx J/\sigma$. This result is unusual. It is not captured, for example, by simple models of river networks (24) that also display some channeling. We are not aware of any alternative theory making such a prediction. As J increases, scaling breaks down, and $P(\sigma)$ becomes peaked both in experiments and in the model.

Second, the same quantitative agreement is found for the spatial correlations of the channel strength C_T and C_L, as shown in Fig. 5: There are, essentially, no correlations in the transverse direction (except at small distances and large J), but correlations are long-range and decay as $1/\sqrt{\Delta y}$ at small J, where Δy is the distance between two sites along the flow direction.

Conclusion

We have shown, experimentally, that, near the erosion onset, the flow of particles is heterogeneous and concentrates into channels whose amplitude is power-law-distributed. Such channels display long-range correlations in the main direction of flow, but no correlations in the transverse direction.

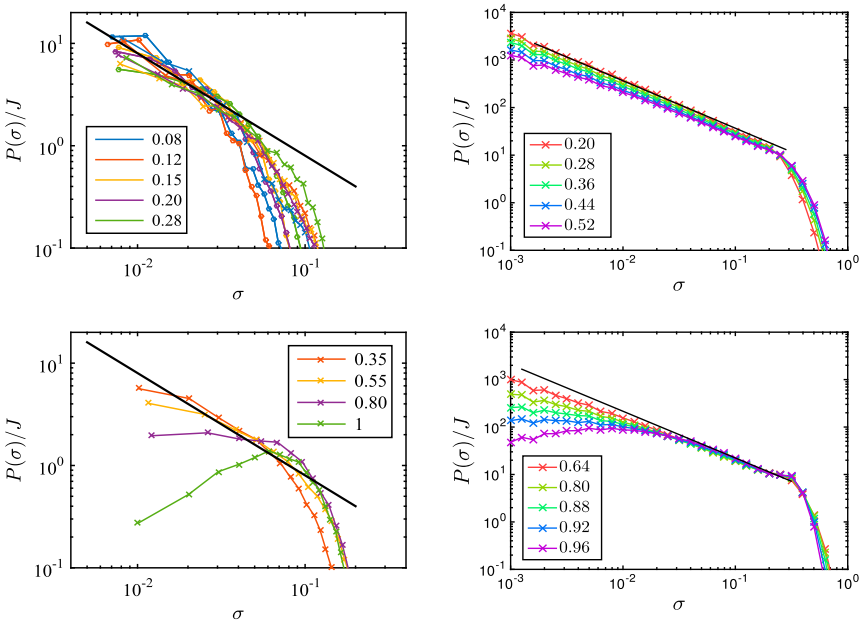

Fig. 4. Probability density of local fluxes $P(\sigma)/J$ for (*Upper*) small flux J and (*Lower*) large J: (*Left*) experiments using the water–UCON mixture (×) and pure water (○) and (*Right*) the theoretical model. The values in the legend are J/J_{max}, and the black solid lines scale as σ^{-1}.

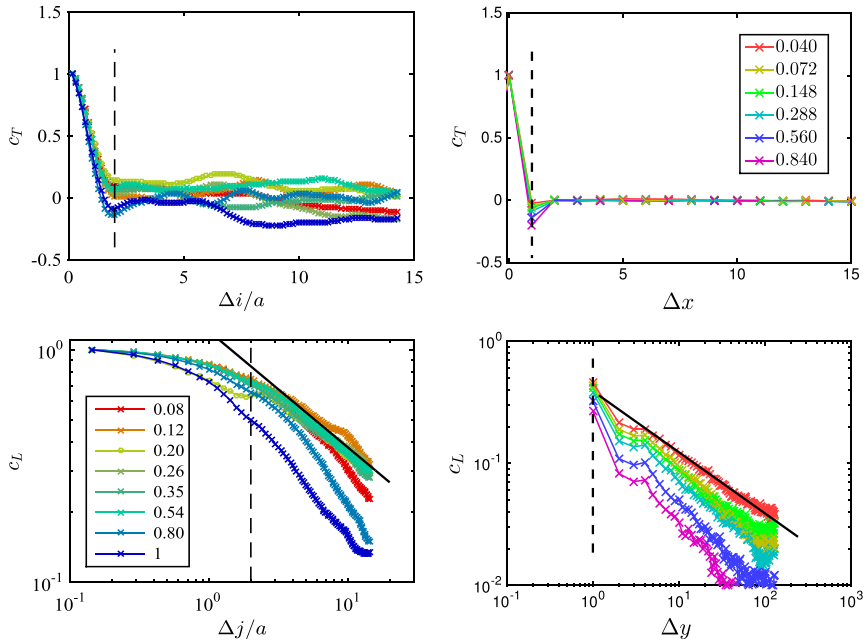

Fig. 5. (*Upper*) Transverse $C_T(\Delta j)$ and (*Lower*) longitudinal correlations $C_L(\Delta i)$ for various J: (*Left*) experiments including both data for water–UCON mixture and water and (*Right*) model. The black dashed lines indicate the distance $2a$ in the experiment and one lattice constant in the model. The black solid lines show $(\Delta j/a)^{-0.5}$ in the experiment and $\Delta y^{-0.5}$ in the model, where the space is measured in the unit of the lattice constant.

These observations agree with a model where the particle dynamics is controlled by the disorder of the bed of static particles, as well as by local interactions between mobile particles. This quantitative agreement suggests that effects ignored in the model are irrelevant (in the sense of critical phenomena) near the transition, at least for the regime of flow reported here; this includes long-range hydrodynamic interactions, as well as the very slow creep flow of the granular bed below the mobile particles (10). Larger experiments, in which a broader range of length and time scales can be probed, would be extremely useful to measure exponents very precisely and settle these issues.

In the framework that emerges from our work, the interplay between disorder and interactions leads to a dynamical phase separating between an arrested phase and a flowing one. The transition is continuous, as supported by the scale-free channel organization near threshold reported here. Generally, near such transitions, the dynamics is expected to be singular, and, indeed, the model predicts $J \approx (\theta - \theta_c)^{\beta}$, with $\beta = 1$ (11). This exponent is consistent with previously experimentally reported values, but precise data accurately measuring β would be very valuable to test this theory further.

Finally, the proposed framework supports a direct comparison between the erosion threshold and other dynamical systems where interacting particles are driven in a disordered environment (13, 14, 25, 26). A classical example is type II superconductors in which the disorder is strong enough to destroy the crystallinity of the vortex lattice (13–15). If the forcing (induced by applying a magnetic field) is larger than some threshold, vortices flow along certain favored paths, reminiscent of the dynamics reported here (13), a phenomenon referred to as "plastic depinning," which is not well understood theoretically (15). Previous theoretical models of this phenomenon (14) did not consider that the interaction between particles can deviate them from their favored path. Such models lead to channels whose amplitude σ is zero or 1 [i.e., $P(\sigma)$ is the sum of two delta functions], at odds with the broad distribution reported here. It would be very interesting to check if our framework applies to plastic depinning in general, by testing, as we have done here, if the distribution of channel strength is, indeed, power law, or is bimodal.

Methods

Experiment. The experimental measurements are performed in a channel test section of length $L = 150$ mm and width $W = 40$ mm, located at a distance of ~500 mm from the channel entrance. This test section is illuminated from below by a homogeneous light and is imaged from above by a digital camera (Basler Scout) with a resolution of 1,392 × 1,040 pixels (Fig. 1). For a given run, typically three to four sequences of typically 300 images are recorded. Note that the different sequences correspond to different decreasing bed heights and thus to different decreasing particle fluxes J until cessation of motion is

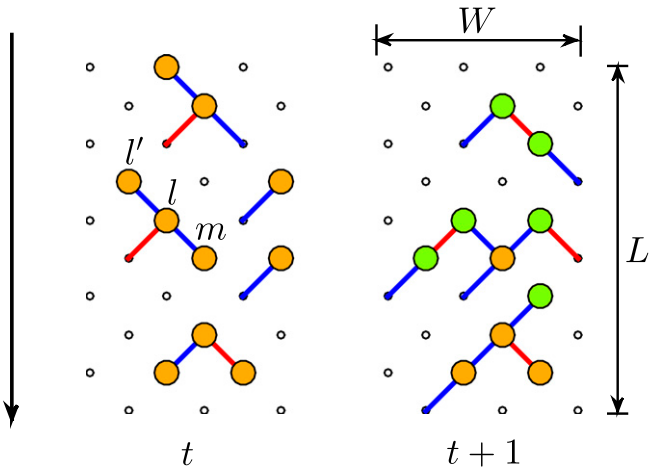

Fig. 6. Illustration of the model, embedded on a square lattice of length L and width W. At each moment, each lattice site indicated by a small circle can accommodate, at most, one particle, represented by a disk. The black arrow along the square diagonal indicates the downstream direction. Solid lines extended from the particles infer the outlets with positive forces. The outlet of the larger force is shown in blue, and the smallest is shown in red. The green discs show the particles moved from the step (*Left*) t to (*Right*) $t+1$.

reached. The images are recorded at a rate of 30 frames per second for water and at a rate of 3.75 frames per second for the water–Ucon mixture. Note that the duration necessary to record a sequence of experimental images is typically of the order of 10 to 100 s, whereas the time necessary for the system to reach the erosion threshold corresponds to several hours. These two time scales are different enough to ensure that sediment transport is in quasi-steady state during an experimental movie. The number of images N that is eventually processed is chosen so as to correspond to a traveled length of 193 mm, i.e., $N = 160$ for water and $N = 257$ for the water–Ucon mixture. These images are then processed to infer real-time positions and velocities of the moving particles. First, for each image of a given sequence, the moving median gray-level image is calculated over a subset of 11 images surrounding the given image (the five preceding and following images in addition to the given image). This moving median image is then subtracted from the given image. This provides a new image that only highlights the moving particles. Second, a convolution of this new image is performed with a disk having the same size as the particles. The resulting maximum intensities yield the centers of the moving particles. Particle trajectories and velocities are finally calculated by using a simple particle-tracking algorithm that relied on the small displacement of the tracked particles between two sequential images by imposing an upper bound condition on particle displacement. Note that these conditions depend on the direction, i.e., the downstream and lateral bounds are smaller than the upstream bound.

Model. Particles interact when they are adjacent. We denote by f the unbalanced force acting on one particle, coming both from particles above it (if they are present) and from a combination of gravity and forcing. The force vector is decomposed into two scalar components along the two outlets: The component $f_{l\to m}$ on bond $l \to m$ is determined by

$$f_{l\to m} = \max(f_{l'\to l} + \theta_{l\to m} + \theta, 0), \quad [6]$$

where $f_{l'\to l}$ is the unbalanced force on particle l' in the direction of the bond $l' \to l$, in the same direction as $l \to m$, as depicted in Fig. 6. If the site l' is empty, $f_{l'\to l} = 0$. That term $f_{l'\to l}$ captures that, if a particle pushes on another one below, the latter has a stronger unbalanced force in that direction. The term $\theta_{l\to m} + \theta$ characterizes the strength of the forcing with respect to the inclination of the link $l \to m$.

From a given state at time t, we first compute all of the forces, illustrated by the red and blue lines in Fig. 6. Then particles that present nonzero unbalanced forces will move in the direction where the force is greatest, if that site below is empty. In practice, we start from the bottom row. For each row, the particles are moved to the unoccupied sites in the row below, starting from the largest unbalanced forces $f_{l\to m}$. Rows are updated one by one toward the top of the system. In our model, we use periodic boundaries. After all L rows (each of width W) have all been updated, time t increases to $t + 1$.

For a given Shields number θ, we initialize the system with particles randomly positioned and study dynamic quantities in the steady state $t \to \infty$. In practice, we average the properties in $t \in [LW, 2LW]$. Our results are shown for $L = 256$ and $W = 64$.

ACKNOWLEDGMENTS. We thank B. Andreotti, D. Bartolo, P. Claudin, E. DeGiuli, and J. Lin for discussions. M.W. thanks the Swiss National Science Foundation for support under Grant 200021-165509, the Simons Collaborative Grant, and Aix-Marseille Université for a visiting professorship. This work is undertaken under the auspices of the Labex MEC (ANR-10-LABX-0092) and of the A*MIDEX project (ANR-11-IDEX-0001-02), funded by the Investissements d'Avenir French Government program managed by the French National Research Agency (ANR).

1. Buffington JM, Montgomery DR (1997) A systematic analysis of eight decades of incipient motion studies, with special reference to gravel-bedded rivers. *Water Resour Res* 33(8):1993–2029.
2. Charru F, Mouilleron H, Eiff O (2004) Erosion and deposition of particles on a bed sheared by a viscous flow. *J Fluid Mech* 519:55–80.
3. Loiseleux T, Gondret P, Rabaud M, Doppler D (2005) Onset of erosion and avalanche for an inclined granular bed sheared by a continuous laminar flow. *Phys Fluids* 17(10): 103304.
4. Ouriemi M, Aussillous P, Medale M, Peysson Y, Guazzelli É (2007) Determination of the critical shields number for particle erosion in laminar flow. *Phys Fluids* 19(6): 061706.
5. Derksen JJ (2011) Simulations of granular bed erosion due to laminar shear flow near the critical shields number. *Phys Fluids* 23(11):113303.
6. Kidanemariam AG, Uhlmann M (2014) Interface-resolved direct numerical simulation of the erosion of a sediment bed sheared by laminar channel flow. *Int J Multiphase Flow* 67:174–188.
7. Ouriemi M, Aussillous P, Guazzelli É (2009) Sediment dynamics. Part 1. Bed-load transport by laminar shearing flows. *J Fluid Mech* 636:295–319.
8. Bagnold R (1966) An approach to the sediment transport problem from general physics. *US Geol Surv Prof Pap* 422:1–37.
9. Chiodi F, Claudin P, Andreotti B (2014) A two-phase flow model of sediment transport: Transition from bedload to suspended load. *J Fluid Mech* 755:561–581.
10. Houssais M, Ortiz CP, Durian DJ, Jerolmack DJ (2015) Onset of sediment transport is a continuous transition driven by fluid shear and granular creep. *Nat Commun* 6:6527.
11. Yan L, Barizien A, Wyart M (2016) Model for the erosion onset of a granular bed sheared by a viscous fluid. *Phys Rev E Stat Nonlin Soft Matter Phys* 93(1):012903.
12. Parker G, Wilcock PR, Paola C, Dietrich WE, Pitlick J (2007) Physical basis for quasi-universal relations describing bankfull hydraulic geometry of single-thread gravel bed rivers. *J Geophys Res: Earth Surf* 112(F4):F04005.
13. Kolton AB, Domínguez D, Gronbech-Jensen N (1999) Hall noise and transverse freezing in driven vortex lattices. *Phys Rev Lett* 83(15):3061–3064.
14. Watson J, Fisher DS (1996) Collective particle flow through random media. *Phys Rev B Condens Matter* 54(2):938–954.
15. Reichhardt C, Reichhardt CJ (2016) Depinning and nonequilibrium dynamic phases of particle assemblies driven over random and ordered substrates: A review. arXiv: 1602.03798.
16. Reichhardt C, Ray D, Reichhardt CJ (2015) Collective transport properties of driven Skyrmions with random disorder. *Phys Rev Lett* 114(21):217202.
17. Phillips CB, Jerolmack DJ (2016) Self-organization of river channels as a critical filter on climate signals. *Science* 352(6286):694–697.
18. Seizilles G, Devauchelle O, Lajeunesse E, Métivier F (2013) Width of laminar laboratory rivers. *Phys Rev E Stat Nonlin Soft Matter Phys* 87(5):052204.
19. Seizilles G, Lajeunesse E, Devauchelle O, Bak M (2014) Cross-stream diffusion in bedload transport. *Phys Fluids* 26(1):013302.
20. Lajeunesse E, Malverti L, Charru F (2010) Bed load transport in turbulent flow at the grain scale: Experiments and modeling. *J Geophys Res: Earth Surf* 115(F4):F04001.
21. Durán O, Andreotti B, Claudin P (2014) Turbulent and viscous sediment transport—A numerical study. *Adv Geosci* 37(37):73–80.
22. Cassar C, Nicolas M, Pouliquen O (2005) Submarine granular flows down inclined planes. *Phys Fluids* 17(10):103301.
23. Boyer F, Guazzelli É, Pouliquen O (2011) Unifying suspension and granular rheology. *Phys Rev Lett* 107(18):188301.
24. Dhar D (2006) Theoretical studies of self-organized criticality. *Physica A* 369(1):29–70.
25. Reichhardt C, Olson CJ (2002) Colloidal dynamics on disordered substrates. *Phys Rev Lett* 89(7):078301.
26. Pertsinidis A, Ling XS (2008) Statics and dynamics of 2D colloidal crystals in a random pinning potential. *Phys Rev Lett* 100(2):028303.